TELKOMNIKA, Vol. 11, No. 9, September 2013, pp. 5245~5252
ISSN: 2302-4046

Linear Modelling for Spectral Images based on Truncated Fourier Series

Qiao Chen[1], Songhua He*[2], Xiangyang Xu[1], Bo Li[1]
[1]School of Media and Communication, Shenzhen Polytechnic, Shenzhen, 518055, China, telp/fax: +86755-26731023/26731837
[2]Institute of Light Science and Technology, NanJing Forestry University, NanJing, 210037, China, telp/fax: +86-13725563936/755 26731837
Corresponding author, e-mail: hdh1818@szpt.edu.cn[2], qiaochen@szpt.edu.cn[1]

Abstract

Reflectance spectra of hyperspectral images of the natural scenes are supposed to represent the real world better than any certain classes of natural and man-made spectral reflectance. But spectral images contain a large volume of data and place considerable demands on computer hardware and software compared with standard trichromatic images. Although principal component analysis (PCA) based low-dimensional linear models have been widely used in spectral image encoding and compression, there is no a single PCA linear model derived from one data set can be guaranteed to accurate represent other data sets. In this study, we proposed a spectral image encoding method by a single linear model constructed by truncated Fourier series, in which a limited number of parameters that is proportional to the highest frequency cut off if the low-pass hypothesis is valid for any of the data sets. In this paper, several groups of hyperspectral images have been processed using truncated Fourier series, the encoded images are analysed in terms of chromaticity and spectral root mean square (RMS) errors. Results show spectral images can be efficiently compressed when the frequency reach a certain limit, and the color information can be well preserved.

Keywords*: spectral image, truncated fourier series, linear model*

1. Introduction

The use of spectral imaging can fundamentally solve the problem of metamerism caused by trichromatic-imaging systems, but at the same time require not only measurements of RGB values, but the spectral information for each pixel of an image. In most cases, multispectral imaging systems use 6 or more broadband sensors, whereas, hyperspectral imaging systems are typically consist of 31 or 61 channels (which, for example, measure at every 10 nm or 5 nm interval in the visual spectrum). Hyperspectral imaging systems have been extensively used for both territorial and remote-sensing applications, where each individual band usually has a spectral resolution of 1 to 20 nm, and spectral sensitivity generally ranges from 350 nm (blue visible) to 2500 nm (thermal infrared) depending on applications [1-3]. During the past few years, hyperspectral imaging has also been introduced to new application areas such as paper industry, art painting, ceramic tile quality control, etc. [4, 5]. But spectral images whose each pixel contains full information of spectral reflectance provide a huge volume of redundant data for the purposed of color reproduction, it is therefore highly desirable to find a way to represent spectral images efficiently by compressing them into a more compact form. It is known any spectral reflectance distribution $P(\lambda)$ can be approximated to a specified degree of accuracy as a weighted sum of basis functions $B(\lambda)$, thus

$$P(\lambda) = a_1 B_1(\lambda) + a_2 B_2(\lambda) + \cdots + a_n B_n(\lambda) \quad (1)$$

Where $P(\lambda)$ is the reflectance spectrum, $B_i(\lambda)$ is the *ith* basis function and a_i is the coefficient or weight for the ith basis function. Once the $B_i(\lambda)$ are known, a set of weights a_i is sufficient to specify any reflectance spectrum in the model. It has been stated that spectral reflectance of surfaces and spectral power distributions of illuminants are highly constrained [6-

Received April 3, 2013; Revised June 9, 2013; Accepted June 20, 2013

8], therefore they can be approximated by low-dimensional linear models of limited weighted sum of basis functions [9-11]. PCA technique has been widely used to derive basis functions, which are orthogonal with each other. The linear model based on PCA is supposed to be the most efficient representation of the original reflectance spectra, but only valid when PCA are applied on the same data sets. It has been stated that if one set of reflectance spectra needs a linear model of N parameters to represent, and another set needs a linear model of M parameters to represent, the adequate number of parameters for a linear model to represent the combined sets will be anywhere between max(M,N) and M+N [12, 13]. This suggests that there is not a single PCA linear model derived from one data set can be guaranteed to accurate represent other data sets. However, since the low-pass property of spectral reflectance makes it possible that a set of spectral reflectance spectra can be represented by a linear model of a small number of parameters, if the number of parameters by frequency limits for the two data sets are M and N respectively, the number of parameters for the combined set will be max (M,N). This suggest all data sets can be fitted appropriately by a single linear model (truncated Fourier linear model) with a limited number of parameters that is proportional to the highest frequency cut off if the low-pass hypothesis is valid for any of the data sets.

The physical constraints of spectral reflectance lead to low-pass hypothesis for spectral reflectance. The studies of frequency limited functions proposed a hypothesis that the spectral reflectance are frequency-limited and low-pass functions [14-17] based on the physical properties of smooth reflectance spectra of most material surfaces. Fourier analysis decomposes a signal into a set of sinusoidal components represented by a phase spectrum and an amplitude spectrum. For a reflectance function $P(\lambda)$, the discrete Fourier transform (DFT) as a expansion of Fourier series as:

$$P(\lambda) = a_0 + \sum_{n=1}^{\infty} a_n \cos(w_n \lambda) + b_n \sin(w_n \lambda) \quad (2)$$

Where for any non-negative integer n, $w_n = n\frac{2\pi}{T}$ is the *nth* harmonic (in radians) of the reflectance function *P*, while a_n and b_n are the even Fourier coefficients and odd Fourier coefficients respectively, *T* is the period of the signal and usually *T*=300 nm in the range of 400 nm to 700 nm. A relation exists between the Fourier frequency limitation (band limit) of a collection of signal and the number of significant independent samples required to represent the signal in the collection. This relationship can be expressed as:

$$N=(2fT)+1 \quad (3)$$

Where (x) stands for the highest integer number smaller than x, and f is the band limit and T is signal extent, which in the case of spectral reflectance, f is in cycles per nanometre, and T is 300 nm. If a band limit of 0.01 cyc/nm is selected, the number of independent samples N of 7 is obtains, which means the range of integer n of Equation (3) will equals (N-1)/2=3. Thus the truncated Fourier series of 7 basis functions are used as a linear model to approximate the original reflectance spectra as Equation (4):

$$\begin{aligned} P(\lambda) &= a_0 + a_1 \cos(\frac{2\pi}{T}\lambda) + a_2 \sin(\frac{2\pi}{T}\lambda) + a_3 \cos(\frac{4\pi}{T}\lambda) \\ &+ a_4 \sin(\frac{4\pi}{T}\lambda) + a_5 \cos(\frac{6\pi}{T}\lambda) + a_6 \sin(\frac{6\pi}{T}\lambda) \end{aligned} \quad (4)$$

Although it is obvious that mathematically a PCA based linear model which is the optimal model to represent the spectra data set will always be more efficient than a truncated Fourier linear model, the truncated Fourier linear model can be more independent. As a universal single linear model, it is important to determine the band limit of the truncated Fourier model when the model is used to represent spectral reflectance. In this work, spectral reflectance data sets from hyperspectral images were formed, and the truncated Fourier model was applied to each data set as an encoding of spectral information. The objective of this study

is to evaluate the performance of using the truncated Fourier linear model to represent spectral images.

2. Research Method

In this work, we collect several groups of spectral images which are consisted of a set of forest and coral images [18], a set of indoor images [19] and a set of natural and indoor images [20, 21]. According to their image contents, 6 image groups are classified into Forest, Coral, Rural, Urban, Flower and Man-made. Forest and Coral image groups contain 12 forest and 10 coral images respectively. Forest images consist of objects include trees, grass, leaves, rock and soil, while Coral images only consist of various corals. Rural images include 3 images (resolution varies from 663×721 pixels to 700×820 pixels) of rural scenes in the Minho region of Portugal, each containing rocks, trees, leaves, grass, and earth. Urban images contain 4 images of urban scenes (three are in similar resolution from 681×418 pixels to 700×608 pixels, one is in resolution of 1017×1340 pixels), from the cities of Porto and Braga, Portugal, which include various buildings and small amount of trees. Flower images consist one red flower (460×460 pixels), one yellow flower (1019×1337 pixels) and a smaller amount of leaves. Man-made images contain indoor scenes (one 820×810 pixels, five 250×250 pixels), which consist of objects including fabric, colour chart, paper, plastic, etc. The Forest and Coral images have a spectral dimension of 40, and images for all other groups have a spectral dimension of 31 (in the range of 400-700 nm and sampled at 10 nm intervals). Each image contains a large volume of data (for example, one forest image contains 128×128×31 values). In order to reduce the computational complexity, only 1024 pixels are randomly selected from each image, and the chosen reflectance sets of each image group are combined together to form a large reflectance spectra set which represents the particular class of scenes (this is possible because one object is composed of many pixels which all have identical or similar spectral reflectance). This method has been applied to all image groups except for Man-made. For the Man-made image group 1024 pixels were randomly selected from all 5 small images (250×250 pixels) and another 1024 pixels were randomly selected from the large image (820×810 pixels). The reason to do this is to balance the occurrence of reflectance in each different scene, since those 5 small images were derived from a larger hyperspectral image which captured one scene, their reflectance spectra are considered to be a single set rather than 5 separated sets. In this study, a set of uniform surface spectra was also considered for comparison. It is a set of 1269 Munsell samples [14] each measured between 400 nm and 700 nm at 10 nm intervals.

For each spectral reflectance function, a DFT was performed using the *fft* function available in Matlab. The proportion of spectral energy below a certain frequency is represented by the proportion of cumulative power in that spectrum, which can be calculated by dividing the sum of power of each frequency by the total cumulative power in that spectrum. Figure 1 illustrates the process of calculating the proportion of the cumulative power for one Munsell reflectance sample. Because the sampling wavelength is 400 nm to 700 nm at 10 nm, the sampling resolution of 31 results in a Nyquist frequency of 15 cycle per 300 nm, so the range of frequency content is from 0 to 15 cyc/300 nm at 1 cyc/300 nm intervals (0 to 0.05 cyc/nm at 0.0033 cyc/nm intervals) as shown in Figure 1. For the Forest and Coral reflectance spectra, which have a sampling resolution of 40 across the wavelength of 400nm to 700nm, the range of frequency content is from 0 to 20 cyc/300 nm at 1 cyc/300 nm intervals (0 to 0.06667cyc/nm at 0.0033cyc/nm intervals).

As mentioned by other authors, most of the reflectance spectra have a null or residual amount of energy in the short wavelength but have a high level, if not a maximum of energy at 700nm, any difference between the values of the spectra at the two ends introduces spurious, high frequency components into the power spectrum. To attenuate these artifacts, a Hanning window function was used to multiply to the original spectral reflectance before it was transformed to the Fourier domain. The Hanning window has very little energy above 2 cyc/300nm, for the windowed version, the discarded energy above a certain frequency which is equal or higher than 2 cyc/300nm will be belong to spectral reflectance, while for frequency limit is less than 2 cyc/300nm, the discarded energy includes both Hanning window and spectral reflectance which can not be separated. The power spectra after applying Hanning window are of poor quality, but the intention is to obtain an overall estimation of power in various parts of the power spectrum, which is possible in spite of the obvious smearing.

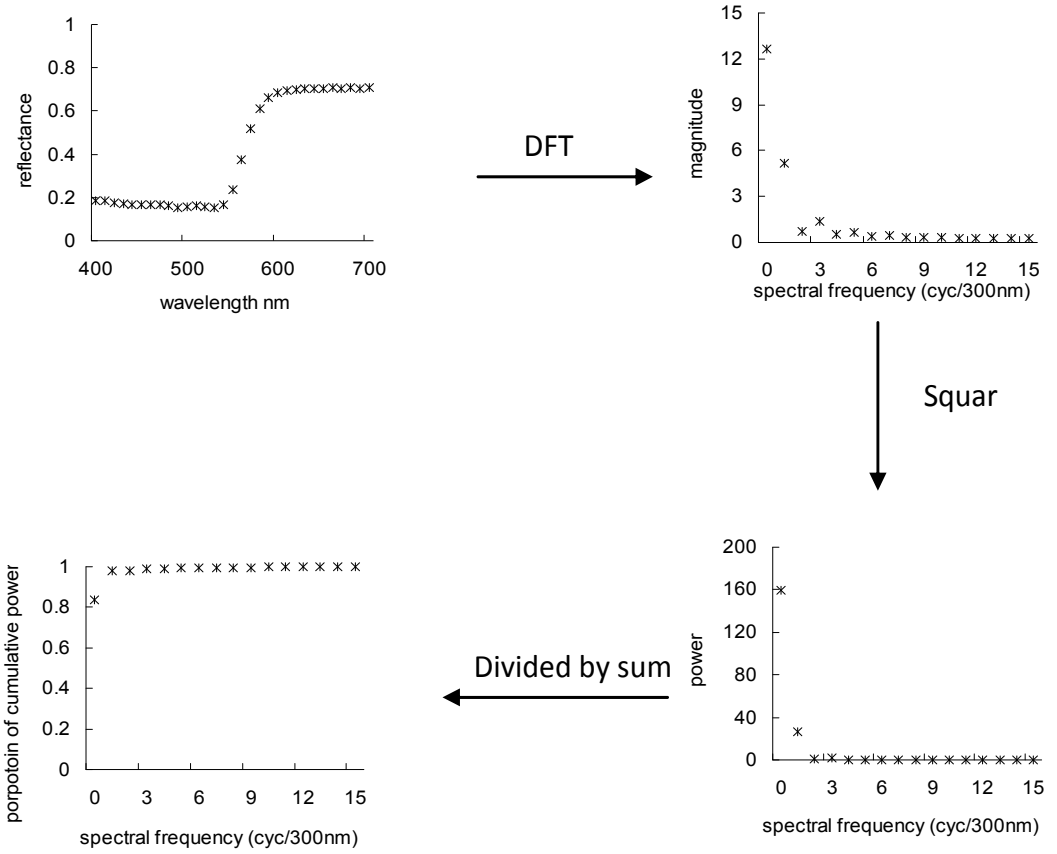

Figure 1. Procedure for Calculating the Proportion of Spectral Energy below Particular Frequency Limit (cyc/300nm) for One Spectral Reflectance Sample

In our study, the DFT as a truncated Fourier series were used as a linear model to fit the original reflectance spectra of different group data sets by the following form:

$$P(\lambda) = c_0 + c_1 \cos(2\pi f_1 \lambda) + c_2 \sin(2\pi f_1 \lambda) + c_3 \cos(2\pi f_2 \lambda) + c_4 \sin(2\pi f_2 \lambda) \ldots + c_{n-2} \cos(2\pi f_N \lambda) + c_{n-1} \sin(2\pi f_N \lambda) \quad (5)$$

Where $P(\lambda)$ is the reflectance spectrum, c_i is the coefficient, and f_N is the Nyquist frequency, which satisfies $n=2fNT+1$, where T is the signal extent (usually 300 nm). For any frequency there are two basis functions: a sine and a cosine functions. The number of basis functions increases with the increase of frequency f_i from 1 to f_N, and a truncated serious at i ($0<i<N$) represent a reconstructed reflectance spectrum with a band limit of f_i. In the study, the linear model for spectral reflectance in terms of truncated Fourier series was implemented by making magnitudes of a series frequency to be zero to remove the energy above a certain band limit, an inverse Fourier transfer (*ifft* function available in Matlab) was then applied to obtain the reconstructed reflectance spectrum.

The Hanning window was multiplied to each individual original spectral reflectance before DFT, the reflectance modelled by truncated Fourier series was then divided by the original Hanning window to create the reconstructed reflectance. The chromatic errors between original and reconstructed spectra were calculated in terms of CIELAB ΔE*ab for each band limit from 1 to f_N, and RMS errors were used to evaluate the performance of spectral reconstructions.

3. Results and Discussion

Table 1 lists the average proportion of cumulative power for each of the 7 sets of reflectance spectra. It is obvious that for all sets of reflectance data, with the increasing of band limits, the proportion of cumulative power increases and reaches 100% at a certain frequency which is usually the Nyquist frequency. Although showing a similar trend, different data sets illustrate various degree of change: Flower set shows the largest variation and urban set shows the smallest variation.

Table 1. Average Proportion of Cumulative Power of Corresponding Frequency

Frequency cyc/300 nm	Proportion of cumulative power						
	Forest	Coral	Rural	Flower	Urban	Man-made	Munsell
0	0.7346	0.7492	0.7363	0.6837	0.8011	0.7554	0.7817
1	0.9768	0.9623	0.9780	0.9247	0.9928	0.9269	0.9812
2	0.9931	0.9699	0.9936	0.9582	0.9968	0.9795	0.9971
3	0.9973	0.9729	0.9971	0.9661	0.9977	0.9917	0.9992
4	0.9981	0.9762	0.9989	0.9709	0.9982	0.9942	0.9997
5	0.9985	0.9807	0.9992	0.9739	0.9984	0.9957	0.9998
6	0.9986	0.9825	0.9993	0.9766	0.9987	0.9972	0.9999
7	0.9988	0.9842	0.9994	0.9793	0.9988	0.9979	1.0000
8	0.9989	0.9858	0.9995	0.9820	0.9990	0.9984	1.0000
9	0.9991	0.9872	0.9996	0.9845	0.9991	0.9987	1.0000
10	0.9992	0.9885	0.9996	0.9870	0.9993	0.9990	1.0000
11	0.9993	0.9897	0.9997	0.9895	0.9994	0.9991	1.0000
12	0.9994	0.9910	0.9998	0.9922	0.9995	0.9993	1.0000
13	0.9995	0.9920	0.9999	0.9949	0.9997	0.9995	1.0000
14	0.9995	0.9930	0.9999	0.9975	0.9998	0.9997	1.0000
15	0.9996	0.9940	1.0000	1.0000	1.0000	1.0000	1.0000
16	0.9997	0.9952	****	****	****	****	****
17	0.9998	0.9963	****	****	****	****	****
18	0.9999	0.9974	****	****	****	****	****
19	0.9999	0.9986	****	****	****	****	****
20	1.0000	1.0000	****	****	****	****	****

(**** not available)

Arbitrary percentage of 99% and 99.9% cumulative power level have been selected as criterions, the corresponding band limits for different group data sets were estimated by a linear interpolation of frequency series, and the results are shown in Table 2. The resulting band limits for the non-windowed and windowed cases are fundamentally different for some data sets. It has been mentioned in the literature that straightforward DFT on the spectral reflectance will lead to misestimating of the power spectrum because of the “windowing” effect of the reflectance its own. The result in Table 2 shows the great effects of the “windowing” of reflectance spectra of low frequency such as the Rural and Man-made data sets: without applying Hanning window, the “windowing” effect of spectral reflectance causes unexpected power at high frequency; while after adding Hanning window, the “windowing” effect is reduced, therefore the power spectrum reflects correct percentage of cumulative power.

The Hanning window has the effect of reducing the candidate band limits by reducing the “windowing” effect of spectral reflectance, but it is also noticed that for Munsell set of 99% criterion, there is a little increase. This doesn’t mean the using of Hanning window is wrong. On other hand, it shows the phenomenon that after applying Hanning window, for all data sets the cumulative energy at 0 cyc/300 nm (DC component) is always lower than Non-window vision, and for Munsell set the cumulative energy at both 0 and 1 cyc/300 nm is lower than Non-window vision. This is because Hanning window has a cut of at 2 cyc/300 nm with most energy below 1 cyc/300 nm. Also because the band limit is estimated by a linear interpolation, the resulting band limits which are below 2 cyc/300 nm is not as accurate as band limits estimated beyond 2 cyc/300 nm.

Table 2. Candidate Frequency Band Limits for All Data Sets of both Window and Non-window Versions based on Criterions of 99% and 99.9% Proportion of Cumulative Power

	Proportion of cumulative power			
	99%		99.9%	
Data set	Non-windowed	Windowed	Non-windowed	Windowed
Forest	4.48	1.81	17.33	8.50
Coral	13.33	11.23	19.44	19.29
Rural	9.85	1.77	14.41	4.33
Flower	12.61	11.19	14.76	14.60
Urban	4.92	0.99	13.43	8.00
Man-made	9.18	1.86	14.29	10.00
Munsell	1.11	1.55	8.00	2.90

Apart from the effects of Hanning window, the band limits for different data sets vary a lot with a certain percentage criterion. In most case, Munsell set needs lower frequency than other data sets to recover the same proportion of energy, while Coral and Flower data set need relatively higher frequency limits than the rest of data sets. Figure 2 and Figure 3 illustrate the average reconstruction errors in CIELAB ΔE*ab and RMS errors respectively. In general, the higher frequency chosen, the smaller reconstruction errors produced (both spectral and colorimetrical), with some exceptional cases of CIELAB ΔE*ab of relatively high frequency limits for some data sets, which indicates that linear modelling of truncated Fourier fitting is not adequate to model the chromatic response.

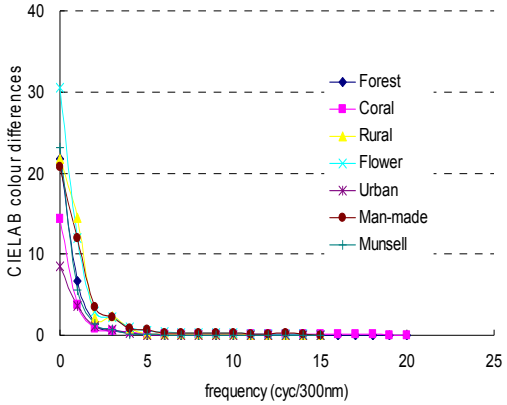

Figure 2. Average CIELAB ΔE^*_{ab} of the 7 Reflectance Data Sets

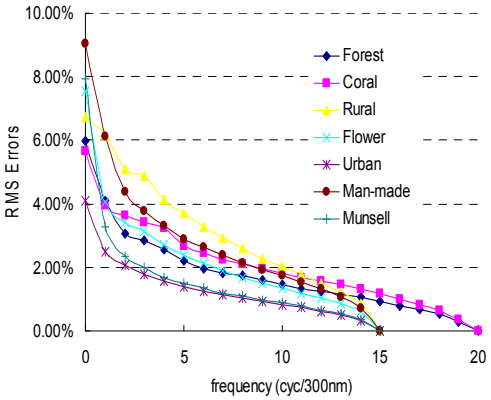

Figure 3. Average RMS Errors of the 7 Reflectance Data Sets

CIELAB ΔE*ab of 1 unit have been selected as a threshold, the corresponding band limits for different group data sets were estimated by a linear interpolation of frequency series, and the results are shown in Table 3. It can be found, for 7 group data sets, a range of band limits from around 2 to 4 cyc/nm will eventually constrain the average CIELAB ΔE*ab to be less than 1. Although reconstruction errors always decrease with the increase of band limits, they are not efficiently optimized in terms of both spectral and colorimetrical errors. For a linear model of truncated Fourier series, the number of basis functions N is determined by equation (6):

$$N_i = 2 f_i + 1 \quad (6)$$

Where f_i is the frequency of 1, 2… to f_N cyc/300 nm of Nyquist frequency, Table 3 also list the corresponding required number of basis functions, which are higher than using PCA based linear modelling.

Table 3. Candidate Frequency Band Limits for All Data Sets based on a Criterion of 1 Unit CIELAB ∆E*ab for Average Reconstructions.

Data set	Band limit	Number of basis functions
Forest	2.50	6
Coral	1.96	5
Rural	3.79	8
Flower	4.02	9
Urban	2.25	6
Man-made	3.86	9
Munsell	2.64	7

4. Conclusion

The frequency analysis of reflectance spectra shows that the low-pass hypothesis are applied to most of the reflectance spectra, except for Flower and Coral data sets, which show a high frequency limit for the cumulative energy below a certain proportion. But all reflectance data sets provide a low band-limit if selecting 1 unit average CIELAB ∆E*ab as the criterion. This result is consistent with the low-pass property of human-visual system that the three classes of cones act as low-pass filters that eliminate frequency higher than 5-6 cyc/300nm. Although the number of linear model of the truncated Fourier series is always larger than the basis function of conventional PCA linear model, it provides an universal model of small number of parameters without the prior knowledge of spectra data sets, and the color information can be well preserved. As far as the low-pass hypothesis is valid for reflectance spectra, this model can be used for any data sets. The further study will be focused on the optimization of the truncated Fourier series linear modelling to minimize visual differences of reconstructed spectral images.

Acknowledgments

This work was supported by National Natural Science Foundation of China (Grant No. 61108087).

References

[1] Ferwerda JG. Charting the quality of forage: measuring and mapping the variation of chemical components in foliage with hyperspectral remote sensing. ITC Dissertation. Wageningen University. 2005.
[2] Hien LP, Kim DS, Eo YD, Yeon SH, Kim SW. *Comparison of Radiometric Pre-processing Methods to Detect Change using Aerial Hyperspectral Images.* IJACT. 2012; 4(9): 1-9.
[3] SHEN D, LI CF, YIN JY. *A Method for Multi-Spectral Remote Sensing Classification Based on Mixed Pixel Analysis.* IJACT. 2012; 4(15): 302-310.
[4] Parkkinen JPS, Jaeaeskelaeinen T. *Spectral imaging.* Proceedings of the International Congress of Imaging Science 2002. Tokyo. 2002: 383-384.
[5] Li CF, Yin JY, Bai CS, Zhao JJ, Ye FY. *An Object-oriented Method for Extracting City Information based on High Spatial Resolution Remote Sensing Images.* IJACT. 2011; 3(5): 80- 88.
[6] Maloney LT. Physics-based approaches to modeling surface color perception. Cambridge University Press. 1999.
[7] Romero J, Garcia-Beltran A, Hermandez-Andrez J. *Linear bases for representation of natural and artificial illuminants.* Journal of the Optical Society of America. 1997; 14(5): 1007-1014.
[8] Owens HC. Color and spatiochromatic processing in the human visual system. PHD Thesis. University of Derby. 2002.
[9] Wu XY, Li YS, Wu CK, Wang L. *Linear Prediction Based Hyper-spectral Imagery Compression Using Distributed Source Coding.* JCIT. 2012; 7(12): 27 - 34.

[10] Kim DS, Pyeon MW. *Aggregation of Hyperion Hyperspectral Bands to ALI and ETM+ Bands Using Spectral Response Information and the Weighted Sum Method.* JDCTA. 2012; 6(5): 189-199.
[11] Peng T, Chen XS, Liu HY, Chen K. *Data Reduction Based on Local Hausdorff Measures for Forensic Data.* JCIT. 2011; 6(5): 273 -279.
[12] Bonnardel V, Maloney LT. Surface spectral reflectances and human chromatic response in the Fourier domain. *Journal of the Optical Society of America.* 2000; 17: 677-686.
[13] Halmos PR. Finite-Dimensional Vector Spaces. New York: Springer-Verlag.1993.
[14] Stiles WS, Wyszecki G, Ohta N. Counting metameric object-color stimuli using frequency limited spectral reflectance functions. *Journal of the Optical Society of America.* 1977; 67(6): 779-784.
[15] Buchsbaum G, Gottschalk A. Chromaticity coordinates of frequency-limited functions. *Journal of the Optical Society of America A.* 1984; 1(8): 885-887.
[16] Gallager RG. Information Theory and Reliable Communication. New York: John Wiley and Sons.1968.
[17] Buchsbaum G, Gottschalk A. *Opponent colours coding and optimum colour information transmission in the retina.* Proceedings of the Royal Society London B. 1983; 220: 89-113.
[18] Chiao CC, Cronin TW, Osorio D. Color signals in natural scenes: characteristics of reflectance spectra and effects of natural illuminants. *Journal of the Optical Society of America A*. 2000; 17(2): 218-224.
[19] Longere P, Brainard DH. *Simulation of digital camera images from hyperspectral input*. Vision Models and Applications to Image and Video Processing. Kluwer. 2001. 123-150.
[20] Nascimento SMC, Ferreira FP, Foster DH. Statistics of spatial cone-excitation ratios in natural scenes. *Journal of the Optical Society of America A*. 2002; 19(8): 1484-1490.
[21] Foster DH, Nascimento SMC, Amano K. *Information limits on neural identification of colored surfaces in natural scences.* Visual Neuroscience. 2004; 21(3): 331-336.